Effects of electron cyclotron current drive on magnetic islands in tokamak plasmas

J. C. Li (李景春),[1] C. J. Xiao (肖池阶),[1,a)] Z. H. Lin (林志宏),[1,2,a)] and K. J. Wang (王凯杰)[1]

[1]*FSC and State Key Lab of Nuclear Physics and Technology, Department of Physics, Peking University, Beijing 100871, People's Republic of China*
[2]*University of California, Irvine, California 92697, USA*

The effects of the electron cyclotron current drive on magnetic islands in tokamak plasmas are studied using gyrokinetic simulations. By investigating the effects of different characteristics of the driven current, such as current density distribution and deposition location, the factors which can determine the suppression effect on the resistive tearing modes have been explored. It is found that an electron cyclotron wave (ECW) driven current with a larger peak value and more focused deposition region has a better stabilization effect. When the ECW-driven current is closer to the rational surface, it has a better stabilizing effect. These gyrokinetic toroidal code (GTC) linear simulations in the electron fluid limit of the tearing modes in the cylindrical geometry agree well with the magnetohydrodynamic codes. Furthermore, the optimal timing control of the current deposition on resistive tearing modes is demonstrated. *Published by AIP Publishing.*
[http://dx.doi.org/10.1063/1.4996021]

I. INTRODUCTION

Tearing modes are one of the major causes of degradation of plasma stability and confinement in tokamaks. They are non-ideal, resonant magnetohydrodynamic (MHD) instabilities, localized around rational flux surfaces. The modes may lead to violent disruptions when they grow non-linearly in size,[1,2] a particularly dangerous phenomenon for a high current tokamak reactor. In particular, neoclassical tearing modes (NTMs),[3,4] a special class of tearing modes, can be triggered by magnetic perturbations, and are expected to limit the plasma pressure well below that predicted by ideal MHD stability. Therefore, tearing modes and their suppression have become one of the vital issues which should be resolved for the stable operation of tokamaks.

So far, several methods for the mitigation and control of tearing modes have been implemented in the existing experiments,[5] the most successful method being the use of an external current drive to suppress the magnetic islands. Electron cyclotron current drive (ECCD) is one of the ways of the external current drive. Since it can be highly localized and robustly controlled, ECCD is considered an effective means of controlling the tearing modes.[6–8] The experimental results of various devices have successfully demonstrated the stabilizing effect.[9–11] Especially, it has been shown that total stabilization of neoclassical tearing modes is possible with co-ECCD in ASDEX Upgrade Tokamak.[12] Active feedback control has also been used to locate islands and drive time-modulated currents as the island rotates.[13]

Theoretically, a generalized Rutherford equation has been used to investigate the influence of the localized current drive.[14–16] Meanwhile, several MHD codes have been developed to study the ECCD suppression of NTM.[17–19] It was found that NTM is stabilized by a continuous radio frequency

(RF) current drive, and the modulated RF current drive that deposits the RF current around the island O-point has a stronger stabilizing effect than a non-modulated one. Nonetheless, some important physics such as kinetic effects on the tearing mode remains an unsolved problem. In high temperature plasmas, kinetic effects, such as orbital effects of both thermal and energetic particles, will play an important role and affect the behavior of the tearing mode.[20,21] To accurately predict the behavior of the tearing mode, more realistic first-principles physics models in the tokamak geometry should be used. In this work, we perform kinetic simulations of the tearing mode by using the gyrokinetic toroidal code (GTC),[22,23] which has been extensively applied to study neoclassical transport,[24] energetic particle transport,[25] microturbulence,[26,27] Alfvén eigenmodes,[28,29] kink modes,[30] and tearing modes.[31] The effects of the localized current drive on the resistive tearing modes (RTMs) have been explored in the GTC simulations.

The remainder of this paper is organized as follows. The physics simulation model of RTM suppression by ECCD is introduced in Sec. II. The driven current characteristics and its mechanism for controlling the magnetic island are presented in Sec. III. Finally, brief conclusions are drawn in Sec. IV.

II. PHYSICS SIMULATION MODEL

The physics model for the simulation of ECCD stabilization in GTC is formulated as follows. For the resistive tearing mode, the electron dynamics can be described by the drift kinetic equation. The time evolution of the electron distribution function f_e reads:

$$\frac{d}{dt}f_e(\mathbf{X}, \mu, v_{\parallel}, t) = \left[\frac{\partial}{\partial t} + \dot{\mathbf{X}} \cdot \nabla + \dot{v}_{\parallel}\frac{\partial}{\partial v_{\parallel}}\right]f_e$$

$$= \left(\frac{\partial}{\partial t}f_e\right)_{collision}, \quad (1)$$

a)Authors to whom correspondence should be addressed: cjxiao@pku.edu.cn and zhihongl@uci.edu

where

$$\dot{\mathbf{X}} = v_{\|}\frac{\mathbf{B}}{B_0} + \frac{c\mathbf{b}_0 \times \nabla\phi}{B_0} + \frac{v_{\|}^2}{\Omega_e}\nabla \times \mathbf{b}_0 + \frac{\mu}{m_e\Omega_e}\mathbf{b}_0 \times \nabla B_0, \tag{2}$$

$$\dot{v}_{\|} = -\frac{1}{m_e}\frac{\mathbf{B}^*}{B_0} \cdot (\mu\nabla B_0 + q_e\nabla\phi) - \frac{q}{m_e c}\frac{\partial A_{\|}}{\partial t}. \tag{3}$$

Here, $\mathbf{X}, \mu, v_{\|}$ is the electron guiding-center position, the magnetic moment and the parallel velocity. A Krook collisional operator, $(\frac{\partial}{\partial t}f_e)_{collsion} = \eta(f_e - f_{e0})$, is used, where f_{e0} is the equilibrium distribution function of the electron. m_e and Ω_e are the electron mass and the cyclotron frequency, and

$$\mathbf{B}^* = \mathbf{B}_0 + \frac{B_0 v_{\|}}{\Omega_e}\nabla \times \mathbf{b}_0 + \delta\mathbf{B}. \tag{4}$$

$\mathbf{B}_0, \delta\mathbf{B}, \phi, A_{\|}$ denote the equilibrium magnetic field, the perturbed magnetic field, the electrostatic potential, and the parallel vector potential, respectively. $\mathbf{b}_0 = \mathbf{B}_0/B_0$ is the unit vector of the equilibrium magnetic field. The equilibrium magnetic field is much larger than the island magnetic field, $\mathbf{B}_0 \gg \delta\mathbf{B}$. Assuming that there is no equilibrium electric field, and $\phi, A_{\|}$ can be written as their perturbed part, $\delta\phi, \delta A_{\|}$, and $\delta\mathbf{B} = \nabla \times \delta A_{\|}\mathbf{b}_0$. We use the toroidal magnetic coordinate system (ψ, θ, ζ), where ψ is the poloidal magnetic flux function, θ is the poloidal angle, and ζ is the toroidal angle. The equilibrium magnetic field can be represented as the covariant form[32]

$$\mathbf{B}_0 = \delta\nabla\Psi + I\nabla\theta + g\nabla\zeta, \tag{5}$$

or the contravariant form

$$\mathbf{B}_0 = q\nabla\Psi \times \nabla\theta - \nabla\Psi \times \nabla\zeta, \tag{6}$$

and the Jacobian is

$$J^{-1} = \nabla\Psi \cdot (\nabla\theta \times \nabla\zeta) = \frac{B_0^2}{gq + Iq}. \tag{7}$$

Assuming a shifted Maxwellian for the equilibrium electron distribution function that satisfies the 0th order electron drift kinetic equation, we can derive the perturbed fluid continuity equation using the electron drift kinetic Eqs. (1)–(3)

$$\frac{\partial}{\partial t}\delta n_e = -\mathbf{B}_0 \cdot \nabla\left(\frac{n_{e0}\delta u_{\|e}}{B_0}\right) - \delta\mathbf{B} \cdot \nabla\left(\frac{n_{e0}u_{\|e0}}{B_0}\right), \tag{8}$$

where $u_{\|e} = u_{\|e0} + \delta u_{\|e}$, the parallel flow is defined as the fluid moments of the corresponding distribution functions, $n_\alpha u_{\|\alpha} = \int dv v_{\|}f_\alpha, n_\alpha = \int dv f_\alpha$; here, the index α=e, i stands for the particle species electron or ion, and the massless electron momentum equation is

$$\frac{\partial\delta A_{\|}}{\partial t} = -c\mathbf{b}_0 \cdot \nabla_{\|}\delta\phi + \frac{c}{n_{e0}e}\mathbf{b}_0 \cdot \nabla\delta p_e + \eta n_{e0}e\delta u_{\|e}. \tag{9}$$

To close the system of the fluid equation, we use the isothermal electron model, i.e., T_e =constant, $p_e = n_e T_e$, then,

$$\delta p_e = \delta n_e T_e + \delta\mathbf{r} \cdot \nabla(n_{e0}T_e). \tag{10}$$

The ions are described by the standard gyrokinetic equation[23]

$$\frac{d}{dt}f_i(\mathbf{X}, \mu, v_{\|}, t) = \left[\frac{\partial}{\partial t} + \dot{\mathbf{X}} \cdot \nabla + \dot{v}_{\|}\frac{\partial}{\partial v_{\|}}\right]f_i = \left(\frac{\partial}{\partial t}f_i\right)_{collision}, \tag{11}$$

$$\dot{\mathbf{X}} = v_{\|}\frac{\mathbf{B}}{B_0} + \frac{c\mathbf{b}_0 \times \nabla\phi}{B_0} + \frac{v_{\|}^2}{\Omega_i}\nabla \times \mathbf{b}_0 + \frac{\mu}{m_i\Omega_i}\mathbf{b}_0 \times \nabla B_0, \tag{12}$$

$$\dot{v}_{\|} = -\frac{1}{m_i}\frac{\mathbf{B}^*}{B_0} \cdot (\mu\nabla B_0 + q_i\nabla\phi) - \frac{q}{m_i c}\frac{\partial A_{\|}}{\partial t}, \tag{13}$$

m_i and Ω_i are the ion mass and the cyclotron frequency, $\mathbf{B}^*$ for ions have the same form as Eq. (4), in which the electron cyclotron frequency is replaced by the ion cyclotron frequency. The collision operator $(\frac{\partial}{\partial t}f_i)_{collision}$ has been implemented in GTC. However, like Ref. 23, we will omit it in this work.

The electrostatic potential ϕ is calculated from the gyrokinetic Poisson equation[23]

$$\frac{4\pi Z_i^2}{T_i}\left(\delta\phi - \delta\tilde{\phi}\right) = 4\pi(Z_i\delta n_i - e\delta n_e). \tag{14}$$

The electron flow $\delta u_{\|e}$ is calculated from the parallel Ampere law

$$\delta u_{\|e} = \frac{c}{4\pi e n_{e0}}\nabla_{\perp}^2\delta A_{\|} + \frac{Z_i n_{i0}}{e n_{e0}}\delta u_{\|i}. \tag{15}$$

The guiding center density of ion n_i and current $u_{\|i}$ can be calculated from the standard gyrokinetic model.[25] The fluid electrons (8)–(10) and the gyrokinetic ions are coupled through the gyrokinetic Poisson equation (14) and Ampere's law (15). These equations form a closed system, which can simulate the low frequency MHD instabilities.

During the ECCD/MHD interaction processes, the momentum transfer rate from the RF field to the electron, F_e^{rf}, could be calculated as Eq. (A4) in Ref. 33

$$F_e^{rf} = \int m_e \mathbf{v}Q(f_e)d^3\mathbf{v}. \tag{16}$$

Here, $Q(f_e)$ is the quasilinear operator, which contains the physics process that electrons are affected by the quasilinear diffusion due to the RF injection. The fluid equation which includes the F_e^{rf} term could give a formalism for modeling the RF-induced ponderomotive force on electrons. Therefore, we incorporate the RF effects by simply adding this term to the electron momentum equation:

$$\frac{\partial\delta A_{\|}}{\partial t} = -c\mathbf{b}_0 \cdot \nabla_{\|}\delta\phi + \frac{c}{n_{e0}e}\mathbf{b}_0 \cdot \nabla\delta p_e + \eta\frac{c}{4\pi}\nabla_{\perp}^2\delta A_{\|} - \frac{F_e^{rf}}{n|q_e|}. \tag{17}$$

We assume that electrons $\mathbf{E} \times \mathbf{B}$ drift cancels with that of ions and neglect the second term of the right hand side of Eq. (15). The term in Eq. (17) is written as:

$$\frac{F_e^{rf}}{n|q_e|} = -\frac{\eta \lambda \mathbf{B} f(\mathbf{r},t)}{\mu_0}. \tag{18}$$

Here, λ has a unit of the inverse length and is associated with the ECCD amplitude, and

$$f(r,t) = \exp\left(-\frac{(r-r_0)^2}{W_{rf}^2}\right) \prod(\xi_0, \Delta\xi_{EC})$$
$$\times \frac{1}{2}\left[\tanh\left(\frac{t-t_0}{t_p}\right) + \tanh\left(\frac{t_0}{t_p}\right)\right], \tag{19}$$

where W_{rf} denotes the characteristic width, r_0 is the central RF deposition point, and $\prod(\xi_0, \Delta\xi_{EC})$ is a square box function for taking into account the wave deposition profile along the helical angle. We define $\prod(\xi_0, \Delta\xi_{EC}) = 1$ for $\xi_{on} < \xi_0 < \xi_{off}$, and $\prod(\xi_0, \Delta\xi_{EC}) = 0$ elsewhere. In our calculations, we set $\xi_{on} = -\pi, \xi_{off} = \pi$, namely, the fast electron source rotates along all the helical angle corresponding to a continuous ECCD in time, and we call this case the non-modulated current drive or continuous current drive.[34] Here, t_0 is an offset time. t_p is the time scale, $t_p \ll \tau_R$, where $\tau_R = a^2\mu_0/\eta$ is the plasma resistive time scale. In this paper, we solve the Eqs. (8)–(15) in the GTC framework, and get the $\delta\phi, \delta A_\parallel$, as well as the magnetic flux, to study the evolution of a magnetic island. The effect of ECCD on the magnetic island is implemented by adding Eqs. (17)–(19). Thus, a resistive electron fluid model is used here, and only the thermal ion is treated as gyrokinetic. Although Alfvén eigenmodes exist in our model, they are stable in our RTM simulations. Note that since the electron fluid equations are based on the drift kinetic equation, our calculations assume that the resistivity is sufficiently large, so that the width of the current layer is much bigger than the electron gyroradius, however, the fundamental condition for gyrokinetic description is satisfied, i.e., $\frac{\omega}{\Omega} \sim \frac{k_\parallel}{k_\perp} \sim \frac{\delta B}{B_0} \sim \frac{e\phi}{T} \sim \varepsilon \ll 1$, where $\omega, k_\parallel$ and $k_\perp$ are the typical frequency, parallel and perpendicular wave numbers of the instability of interest and Ω is the ion cyclotron frequency.

The gyrokinetic particle simulation uses the particle-in-cell (PIC) method to solve the gyrokinetic equation. In order to minimize the Monte-Carlo noise caused by the PIC method, the so-called δf scheme is introduced.[35] We define $\delta f = f - f_0$, where f is the time-evolving distribution function of the system and f_0 is the equilibrium distribution function, which remains fixed and includes the initial density and temperature profiles. Then, the gyrokinetic equation can be rewritten, so that $\delta f/f$ is now evolving in time rather than the full f. This scheme greatly reduces the statistical fluctuations in the calculations. Moreover, a finite element method (FEM)[36] is used to solve the gyrokinetic Poisson equation; this method is efficient for the non-adiabatic electron response, for both the electrostatic and electromagnetic simulations, and is suitable for dealing with complicated geometries. We have a load of 1 000 000 ions for the kinetic calculation. In order to solve the fluid equations, a Runge-Kutta method of second order is used in the time domain and a finite element technique is also adopted in the space domain. Thus, the second-order accuracy is retained in the fluid part of the simulations. The time step size is 1.04×10^{-8} s ($1N$). Since our calculation
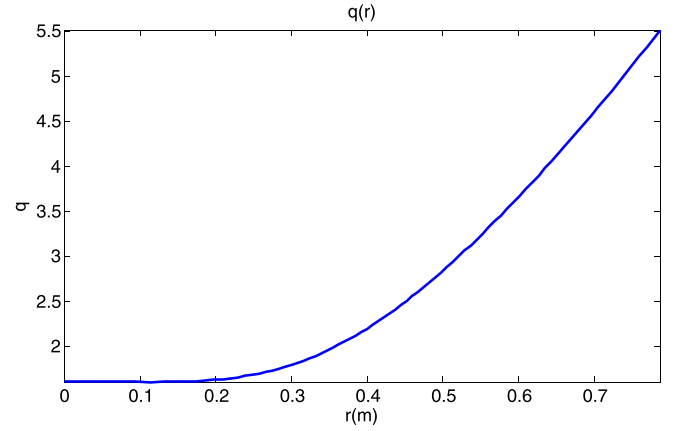

FIG. 1. The safety factor q as a function of minor radius.

is linear, the growth rate of resistive tearing modes becomes constant after 1000 steps. Therefore, 1000 time steps are calculated in our simulations.

III. SIMULATION RESULTS

We investigate the (m/n = 2/1) resistive tearing mode behavior in the cylinder with q = 1.6155–0.327r/R_0+4.232(r/R_0)^2. The other simulation parameters are: the inverse aspect ratio $\varepsilon = r/R_0 = 0.349$ at the rational surface with q = 2/1, the major radius $R_0 = 100$ cm, the magnetic field $B_0 = 1$ T, the equilibrium electron density on the magnetic axis $n_{e0} = 10^{14}$/cm^3, the plasma temperature $T_i = T_e = 100$ eV, the plasma resistivity $\eta = 4.0 \times 10^{-5} \Omega$/m, the electron beta $\beta_e = 0.004$, the magnetic Reynolds number $R_m = 0.8 \times 10^6$, with the initial island width of $0.1a$, and the shape of the initial field perturbation given as -2.632×10^{-3} (r/R_0)^2(1-r/R_0)^2, and the equilibrium safety factor profile is shown in Fig. 1. Figure 2 shows the mode structures of the parallel vector potential $\delta A_\parallel$ and the electrostatic potential $\delta\phi$ on the poloidal plane. In order to verify the GTC capability of the resistive tearing mode simulation, we calculate the radial mode structures with a 1D eigenvalue code and a GTC code with the same input parameter. The results are shown in Fig. 3, which demonstrates that the GTC fluid simulation result agrees well with the eigenvalue result. Therefore, Figs. 2 and 3 have accurately recovered the (2, 1) resistive tearing mode structures.
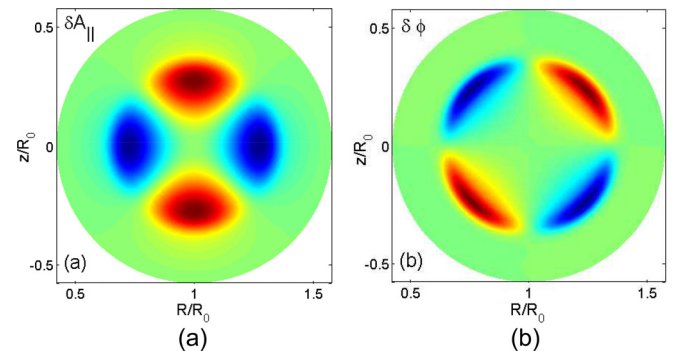

FIG. 2. Mode structures of (a) $\delta A_\parallel$ and $\delta\phi$ (b) from GTC simulation of the (2,1) resistive tearing mode in the cylindrical geometry.
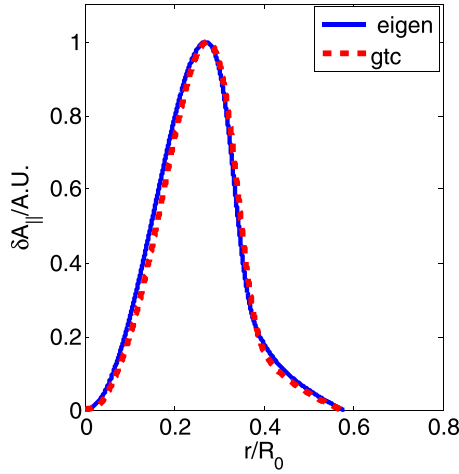
FIG. 3. Comparison of the radial mode structure of the (2, 1) resistive tearing mode between GTC fluid simulation and fluid eigenvalue calculation in the cylindrical geometry.

A. Effect of driven current amplitudes

In order to study the effect of driven current on RTM stabilization, we change the amplitude of the electron cyclotron wave (ECW) driven current with all other parameters being held constant and $W_{rf} = 0.06a$. Figure 4 gives the ECW-driven current density profiles with various peak values. The simulation results are depicted in Fig. 5. It is demonstrated that the m/n = 2/1 magnetic island width at the time step $t = 1000N$ decreases as I_{cd} increases. For a larger I_{cd} (I_{cd} is approximately at $0.04I$, where I is the initial toroidal current), the island width even goes to zero and the magnetic island disappears. We conclude that a larger magnitude of the driven current results in a better suppression and a smaller magnetic island width. This is consistent with the MHD simulations.[18] The island width becomes smaller when ECCD is injected, indicating that the new current density has the stabilization effect, and thus decreases the growth of the island width, even leading to the disappearance of the magnetic island.

B. Effect of deposition profiles

As shown in Eq. (16), a current with a Gaussian distribution is driven by ECW. The stabilization effect depends not
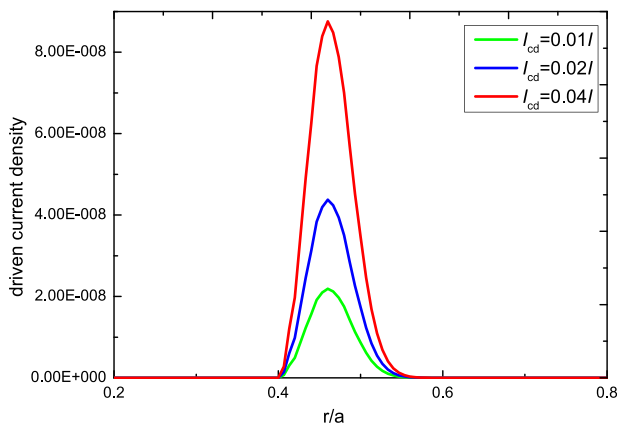

FIG. 4. The ECW-driven current density with different peak values.
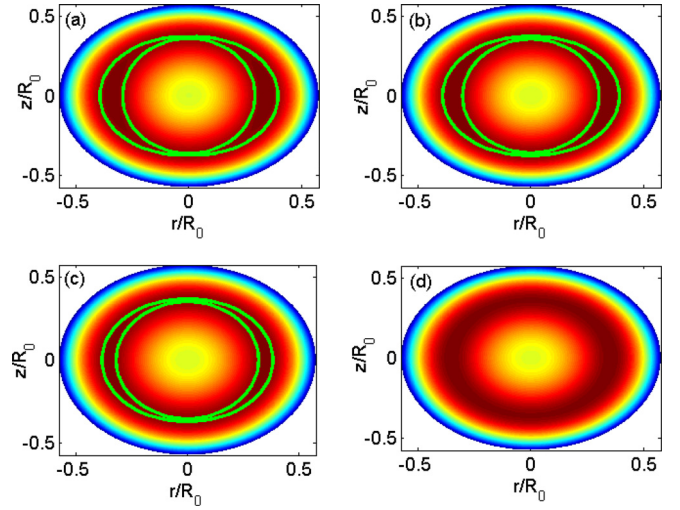

FIG. 5. The magnetic island sizes for different peak values of the current drive: (a) $I_{cd} = 0$, (b) $I_{cd} = 0.01I$, (c) $I_{cd} = 0.02I$, and (d) $I_{cd} = 0.04I$.

only on the current magnitude but also on the deposition width. Thus, it is necessary to study the effect of the deposition region on the RTM suppression. Figure 6 shows the profile of $f(r)$ and the magnetic island width at $t = 1000N$ versus various W_{rf} values: $W_{rf} = 0.06a, 0.10a, 0.14a, 0.16a, 0.18a$, and with $I_{cd} = 0.04I$. Fig. 6 shows that the island width increases with W_{rf}, which means that the stabilizing effect decreases for a larger W_{rf}. The island width has been reduced to zero when the W_{rf} is set as sufficiently small. This result is slightly different from Yu's study,[18] where the island width is not zero. The results indicate that more concentrated ECW-driven current has a better suppression effect. So, for the RTM stabilization, the toroidal injection angle for ECW should be as small as possible in order to get a more localized current profile for a better suppression efficiency.

Due to technical limitations in experiments, it is usually very hard to deposit the ECW-driven current just on the rational surface. So, it is necessary to investigate the dependence of the stabilizing effect on the radial deposition position. Figure 7 shows the relationship between the magnetic island width at $t = 1000N$ and the normalized radial
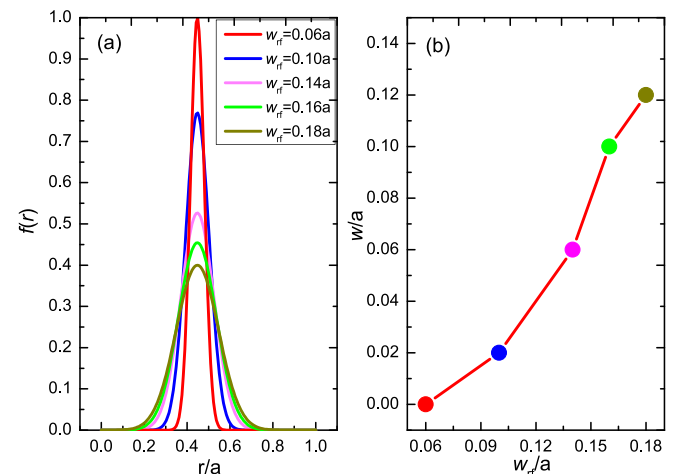

FIG. 6. (a) The profile of $f(r)$, (b) the magnetic island width versus various W_{rf} values.
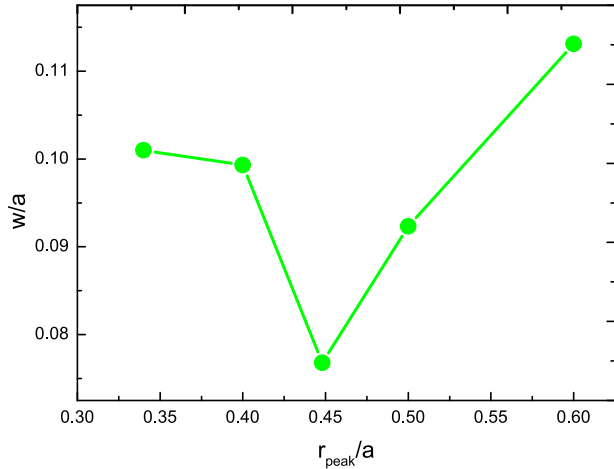
FIG. 7. The magnetic island width vs the normalized radial deposition position of ECW-driven current.

deposition position of the ECW-driven current. Here, $W_{rf} = 0.16a$ and other parameters are the same as in Fig. 6. It is shown that when the ECW-driven current is closer to the rational surface, the stabilizing effect is better.

From these simulations, we can see that the value of current density at the rational surface is the key to the stabilizing resistive tearing mode. Therefore, the ratio of the ECW-driven current density and the plasma current density, $\eta_{RTM} = J_{EC}/J_P$, at the rational surface, can be used as a figure of merit for RTM stabilization. A higher value of η_{RTM}, namely, higher driven current density and narrower driven current density profiles, can enhance the suppression effect. With this figure of merit, criteria for the suppression of resistive tearing modes can be obtained theoretically according to a specific tokamak configuration.[37] It is usually necessary to analyze this criterion, so as to achieve the RTM suppression capacity and propose an optimized construction plan before the installation of the ECW system on tokamaks.

C. Effect of the initial time of deposition

We now study the effect of injection time of the ECW-driven current on the RTM stabilization. Figure 8 shows the
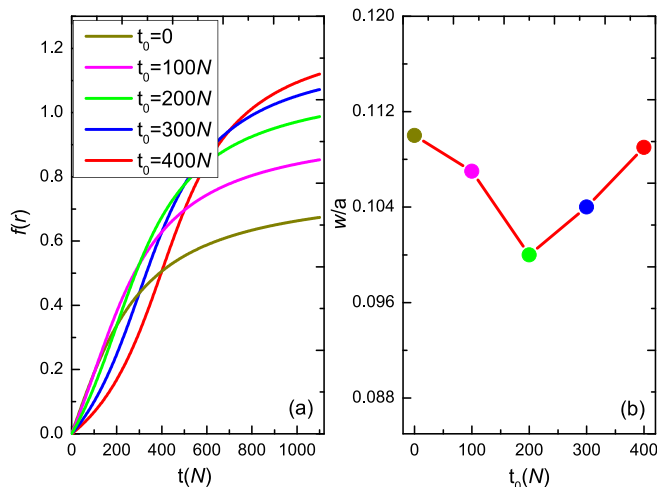

FIG. 8. (a) The profile of $f(r)$, (b) the magnetic island width at $t = 800\,N$ versus various t_0.

profile of $f(r)$ with different t_0 values in Eq. (19), (b) the magnetic island width at $t = 800\,N$ versus various t_0 values, where $I_{cd} = 0.05I$ and $t_p = 250N$.

We can see that the magnetic island width changes little when the t_0 is increased, which means that the effects of the initial time of deposition on the linearly growing islands are minimal in our simulations.

Our results are different from those obtained in Ref. 38, which shows that the stabilization efficiency is better when the current deposition starts at the early phase of resistive tearing mode growth. The reason for this difference may be due to the different ECW-driven current formats we used. From 8 (a), we can see that in order to keep the total current injected into the plasma unchanged, the peak of the profile when $t_0 = 0$ is lower than in the other case, thus, the magnetic island width is almost unchanged with different t_0 values. However, in Ref. 38, the calculations just push forward the initial time of deposition. Therefore, we can conclude that the current deposition that begins at an earlier time does not enhance the suppression efficiency, but the deposition duration should be important to stabilize the resistive tearing mode.

IV. CONCLUSIONS

The effects of the electron cyclotron current drive on magnetic islands in tokamak plasmas are studied using gyro-kinetic simulations. By investigating the effects of different characteristics of the driven current, such as density distribution and deposition location, the factors which can determine the suppression effect on the resistive tearing modes have been explored. It is found that an electron cyclotron wave driven current with a larger peak value and a more focused deposition region has a better stabilization effect. When the ECW-driven current is closer to the rational surface, the stabilizing effect is better. These GTC linear simulations in the fluid electron limit of the resistive tearing modes in the cylindrical geometry agree well with the magnetohydrodynamic codes. Furthermore, the optimal timing control of the current deposition on resistive tearing modes is studied. It is found that the effects of the initial time of deposition on the linearly growing islands are minimal in our simulations. The current deposition that begins at an earlier time does not enhance the suppression efficiency; however, the deposition duration should be important to resistive tearing mode stabilization. Our work will contribute to the development of more comprehensive and precise models for the ECCD-based mitigation and control of neoclassical tearing modes.

[1]G. Giruzzi, M. Zabiégo, T. A. Gianakon, X. Garbet, A. Cardinali, and S. Bernabei, Nucl. Fusion **39**, 107 (1999).

[2]G. Giruzzi, M. Zabiégo, H. Zohm, S. Bernabei, and F. Paoletti, "Review of tearing mode stabilization by RF power in tokamaks," AIP Conf. Proceedings **485**(1), 35–44 (1999).

[3]C. C. Hegna, Phys. Plasmas **5**, 1767 (1998).

[4]R. J. La Haye, Phys. Plasmas **13**, 055501 (2006).

[5]A. Isayama, Y. Kamada, N. Hayashi, T. Suzuki, T. Oikawa, T. Fujita, T. Fukuda, S. Ide, H. Takenaga, K. Ushigusa, T. Ozeki, Y. Ikeda, N. Umeda, H. Yamada, M. Isobe, Y. Narushima, K. Ikeda, S. Sakakibara, K. Yamazaki, K. Nagasaki, and JT-60 Team, Nucl. Fusion **43**, 1272 (2003).

[6]J. C. Li, X. Y. Gong, J. Q. Dong, P. W. Zheng, S. D. Song, Q. D. Gao, and D. Du, Phys. Plasmas **22**, 062512 (2015).

[7]J. C. Li, X. Y. Gong, J. Q. Dong, J. Wang, N. Zhang, P. W. Zheng, and C. Y. Yin, Phys. Plasmas **23**, 122504 (2016).

[8]M. Maraschek, G. Gantenbein, Q. Yu, H. Zohm, S. Günter, F. Leuterer, A. Manini, G. ECRH, and ASDEX Upgrade Team, Phys. Rev. Lett. **98**(2), 025005 (2007).

[9]H. Zohm, G. Gantenbein, G. Giruzzi, S. Günter, F. Leuterer, M. Maraschek, J. Meskat, A. G. Peeters, W. Suttorp, D. Wagner, M. Zabiégo, ASDEX Upgrade Team, and ECRH Group, Nucl. Fusion **39**, 577 (1999).

[10]A. Isayama, Y. Kamada, T. Ozeki, S. Ide, T. Fujita, T. Oikawa, T. Suzuki, Y. Neyatani, N. Isei, K. Hamamatsu, Y. Ikeda, K. Takahashi, K. Kajiwara, and JT-60 Team, Nucl. Fusion **41**, 761 (2001).

[11]C. C. Petty, R. J. La Haye, T. C. Luce, D. A. Humphreys, A. W. Hyatt, J. Lohr, R. Prater, E. J. Strait, and M. R. Wade, Nucl. Fusion **44**, 243 (2004).

[12]G. Gantenbein, H. Zohm, G. Giruzzi, S. Günter, F. Leuterer, M. Maraschek, J. Meskat, Q. Yu, ASDEX Upgrade Team, and ECRH-Group, Phys. Rev. Lett. **85**, 1242 (2000).

[13]R. J. La Haye, S. Günter, D. A. Humphreys, J. Lohr, T. C. Luce, M. E. Maraschek, C. C. Petty, R. Prater, J. T. Scoville, and E. J. Strait, Phys. Plasmas **9**, 2051 (2002).

[14]H. Zohm, Phys. Plasmas **4**, 3433 (1997).

[15]C. C. Hegna and J. D. Callen, Phys. Plasmas **4**, 2940 (1997).

[16]P. H. Rutherford, Phys. Fluids **16**, 1903 (1973).

[17]Q. Yu, S. Günter, G. Giruzzi, K. Lackner, and M. Zabiego, Phys. Plasmas **7**, 312 (2000).

[18]Q. Yu, X. D. Zhang, and S. Günter, Phys. Plasmas **11**, 1960 (2004).

[19]T. G. Jenkins and E. D. Held, J. Comput. Phys. **297**, 427–441 (2015).

[20]H. Cai, S. Wang, Y. Xu, J. Cao, and D. Li, Phys. Rev. Lett. **106**, 075002 (2011).

[21]Y. Liu, R. J. Hastie, and T. C. Hender, Phys. Plasmas **19**, 092510 (2012).

[22]Z. Lin, T. S. Hahm, W. W. Lee, W. M. Tang, and R. B. White, Science **281**, 1835 (1998).

[23]I. Holod, W. L. Zhang, Y. Xiao, and Z. Lin, Phys. Plasmas **16**, 122307 (2009).

[24]W. Zhang, Z. Lin, and L. Chen, Phys. Rev. Lett. **101**, 095001 (2008).

[25]Z. Lin, W. M. Tang, and W. W. Lee, Phys. Rev. Lett. **78**, 456 (1997).

[26]Z. Lin, I. Holod, L. Chen, P. H. Diamond, T. S. Hahm, and S. Ethier, Phys. Rev. Lett. **99**, 265003 (2007).

[27]Y. Xiao and Z. Lin, Phys. Rev. Lett. **103**, 085004 (2009).

[28]H. S. Zhang, Z. Lin, and I. Holod, Phys. Rev. Lett. **109**, 025001 (2012).

[29]Z. Wang, Z. Lin, I. Holod, W. W. Heidbrink, and B. Tobias, Phys. Rev. Lett. **111**, 145003 (2013).

[30]J. McClenaghan, Z. Lin, I. Holod, and W. Deng, Phys. Plasmas **21**, 122519 (2014).

[31]D. J. Liu, W. L. Zhang, J. McClenaghan, J. Q. Wang, and Z. Lin, Phys. Plasmas **21**, 122520 (2014).

[32]R. B. White and M. S. Chance, Phys. Fluids **27**, 2455 (1984).

[33]T. G. Jenkins, S. E. Kruger, C. C. Hegna, D. D. Schnack, and C. R. Sovinec, Phys. Plasmas **17**, 012502 (2010).

[34]X. G. Wang, X. D. Zhang, B. Wu, S. Z. Zhu, and Y. M. Hu, Phys. Plasmas **22**, 022512 (2015).

[35]S. E. Parker and W. W. Lee, Phys. Fluids B **5**, 77 (1993).

[36]Y. Nishimura, Z. Lin, J. L. V. Lewandowski, and S. Ethier, J. Comput. Phys. **214**, 657 (2006).

[37]F. W. Perkins and R. W. Harvey, Bull. Am. Phys. Soc. **45**, 278 (2000).

[38]L. Chen, J. Y. Liu, P. Duan, A. H. Mao, and J. Z. Sun, Phys. Plasmas **21**, 102106 (2014).